



Universiteit
Leiden
The Netherlands

Plasmonic enhancement of single-molecule fluorescence under one- and two-photon excitation

Lu, X.

Citation

Lu, X. (2021, December 8). *Plasmonic enhancement of single-molecule fluorescence under one- and two-photon excitation*. *Casimir PhD Series*. Retrieved from <https://hdl.handle.net/1887/3245677>

Version: Publisher's Version

License: [Licence agreement concerning inclusion of doctoral thesis in the Institutional Repository of the University of Leiden](#)

Downloaded from: <https://hdl.handle.net/1887/3245677>

Note: To cite this publication please use the final published version (if applicable).

5

Two-photon-excited single-molecule fluorescence enhanced by gold nanorod dimers

In this chapter, we demonstrate for the first time two-photon-excited single-molecule fluorescence enhancement by end-to-end self-assembled gold nanorods dimers. We developed a controllable method to create end-to-end gold nanorod dimer structures based on the specific molecular recognition of biotin and streptavidin. The typical size of streptavidin of around 5 nm separates the gold nanorods with gaps suitable for the access of fresh dyes in aqueous solution, yet give very high two-photon fluorescence enhancement. Simulations show that enhancements of more than seven orders of magnitude can be achieved for two-photon-excited fluorescence in the plasmonic hotspots. With such high enhancements, we successfully detect two-photon-excited fluorescence for a common organic dye (ATTO 610) at the single-molecule level.

5.1. Introduction

Two-photon-excited fluorescence is a nonlinear optical process, where a fluorophore simultaneously absorbs two photons of identical frequency, leading to the emission of a photon with higher energy[1, 2]. Ever since its first prediction by Maria Goeppert-Mayer in 1931[3], and its experimental demonstration by Frank et al in the 1960s[4, 5], two-photon excitation has attracted significant interest for several advantages, such as strong background suppression[1], deeper tissue penetration[6, 7], less photodamage to the samples[8, 9], and intrinsic optical sectioning[10–12]. Practical applications of two-photon excitation, however, are limited by the requirement of extremely high photon density. The invention of ultrashort-pulse lasers, has led to a rapid growth of two-photon-based techniques in various scientific fields[10], such as imaging[6, 7, 10–12], microfabrication[13–17] or optical storage[18–21].

Recent progress in nano-optics has made it possible to enhance the two-photon excitation process through near-field confinement by plasmonic nanostructures[22, 23]. The local electromagnetic field around the plasmonic structures can be enhanced by one or more orders of magnitude, depending on their shapes, sizes and the materials. Among all kinds of plasmonic structures, wet-chemically synthesized gold nanorods have been widely exploited in the context of field-enhanced spectroscopy for their facile synthesis and narrow tunable plasmon resonances[24, 25]. In the past few years, gold nanorods have been applied to enhance the fluorescence of single weak emitters[26–29]. Fluorescence enhancements by 3 ~ 4 orders of magnitude have been reported with single nanorods (GNRs) of suitable plasmon resonances, through enhancement of both the excitation and radiative rates of the emitters[26–29]. Higher enhancement factors of about $10^5 \sim 10^6$ have also been achieved in strongly coupled gold nanosphere dimers[30].

Fluorescence upon two-photon excitation is expected to give rise to much larger enhancement than one-photon excited fluorescence due to the quadratic dependence of this process on the excitation intensity[31–35]. The effective enhancing volume under two-photon excitation is restricted to much smaller regions, which improves the sensitivity of detecting the enhanced two-photon-excited fluorescence signals. Single-molecule or single-particle detection of two-photon-excited fluorescence opens up the door to reveal the intrinsic nature of nonlinear interaction between photons and molecules[36], which usually hidden in ensemble experiments. By using a single GNR, we have earlier reported strong two-photon-excited photoluminescence enhancement of single colloidal quantum dots (Qdots), with enhancement factors larger than 10,000-fold[34]. Such high enhancement, however, is still not enough to distinguish the enhanced two-photon-excited fluorescence of single organic molecules from background molecules, which usually have much lower two-photon absorption cross-section than Qdots (about 1000 times smaller). A few other plasmonic structures, such as nanofabricated bow-tie antennas[33], have also been reported to give two-photon enhancement, yet the enhancement factors were even lower than those of GNRs. Oluwafemi et al. have recently demonstrated that two-photon absorption of Rubpy molecules can be enhanced by 10^8 inside the nanoparticle-on-mirror (NPoM) sub-nm cavities[35]. Despite the extremely large enhancement factor, in order to enhance single-molecule two-photon-excited fluorescence, the NPoM structures are limited by i) the requirement of large illumination angles to efficiently excite the cavity modes; ii) photobleaching of the molecules,

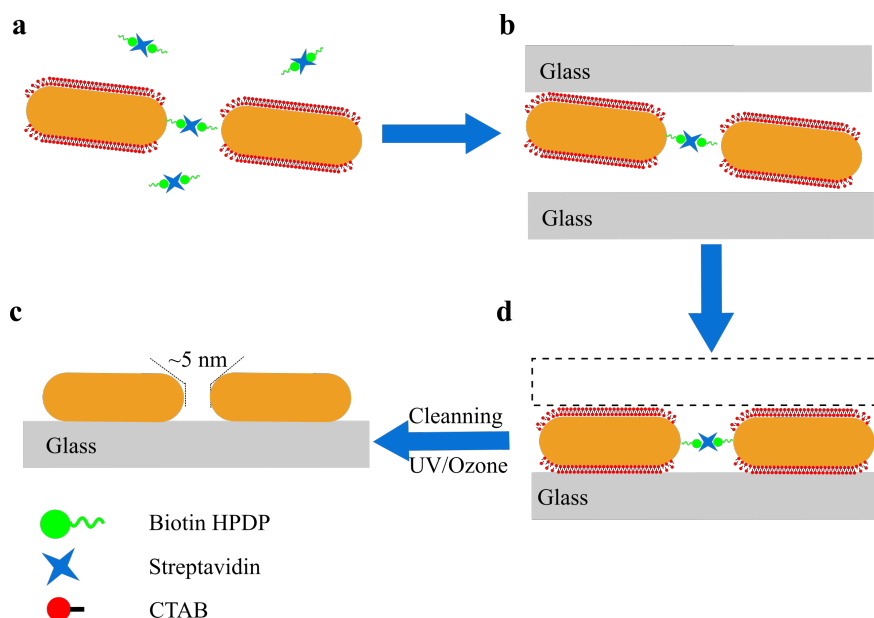


Figure 5.1: Scheme for end-to-end assembly of gold nanorod dimers. (a) Pretreated molecular linkers based on biotin disulfides-streptavidin biomolecular pairs were added to the GNRs solution to trigger the end-to-end assembly of GNRs. (b,d) The assembled GNR dimers were deposited onto a clean glass, which was covered by other glass slides to stop the assembling of GNRs. (c) UV/Ozone cleaning was performed to remove the organic molecules around the GNRs.

which leads to signal loss, as the cavities are not accessible to fresh molecules.

In this work, we demonstrate the first two-photon-excited fluorescence enhancement experiments on single organic fluorophores using end-to-end assembled GNR dimers. The end-to-end assembly was achieved by tip-specific functionalization of the GNRs with molecular linkers. We employed the molecular linkers based on biomolecule pairs consisting of two biotin disulfides bridged by a streptavidin, which ensured an open cavity for single-molecule detection with an interparticle gap of around 5 nm[37]. We applied the GNR dimers to enhance the two-photon-excited fluorescence of commercial organic dyes, which have a broad two-photon absorption band in the infrared range. Theoretical results indicate that two-photon-excited fluorescence enhancement of these molecules can reach 10^7 in the gaps between the GNRs. With such high enhancement factors, we successfully detected enhanced two-photon-excited fluorescence from single molecules.

5.2. Results and discussion

Fig 5.1 schematically illustrates our approach of GNR dimers synthesis. Briefly, a GNR colloid solution (simplified as GNR solution in following) was mixed with the pretreated biomolecular linkers that consisted of at least two biotin disulfides linked with one streptavidin. These molecular linkers were bound to the tips of the GNR through thiol attachment in the present of cetyl(trimethyl)ammonium bromide (CTAB), which occupied more com-

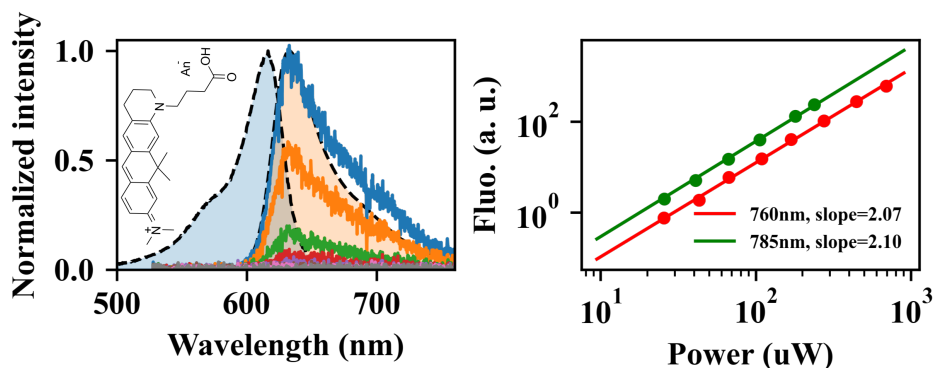


Figure 5.2: Optical characterization of ATTO 610. (a) The blue- and yellow-shaded bands with dashed outline represent the normalized one-photon absorption (blue-shaded) and emission (yellow-shaded) spectra of ATTO 610, respectively. The solid lines give the emission spectra of 4 μM ATTO 610 excited by ~ 220 fs laser pulses at 760 nm with different powers. The integrating time for recording the spectra was set as 120 s. The inset shows the chemical structure of ATTO 610. (b) Power dependence of the emission integrated over wavelengths ranging from 555 nm to 728 nm, excited at the wavelength of 760 nm (red dots) and 785 nm (green dots). The power law fits (solid lines) show perfect quadratic dependence of the emission on the excitation power for both excitation wavelengths.

5

pactly the sides of GNRs, leaving only the tips reactive for the linkers. Therefore, the GNRs were linked by the molecular linker at the ends, leading to the end-to-end assembly of GNRs in the solution (figure 5.1a). We monitored the assembly process by measuring the real-time absorption spectrum of the mixture to ensure most assembled structures to be the end-to-end dimers. A small amount (10 μL) of the assemblies of GNRs were deposited from the solution onto a clean cover glass slide. We stop the assembling by covering the slide with the assembly solution with another clean slide (see figures 5.1b and d). By using this strategy, a very thin film of the assembly solution is formed between the two slides, which dry very quickly, leaving every assembled GNRs sticking on one of the glass slides. We performed UV/Ozone cleaning to remove all the organic molecules around the GNRs to ensure the proper sticking of the GNRs on the glass surface, and to create free gaps between the GNRs of the assemblies.

We performed two-photon-excited single-molecule fluorescence experiments on a commercial dye called ATTO 610 (ATTO-TEC) enhanced by the GNR dimer structures. ATTO 610 is a bright dye with high photostability under one-photon excitation. It has a one-photon absorption maximum at 616 nm and an emission maximum at 633 nm. ATTO 610 also exhibits two-photon absorption in the infrared range under illumination with ultrashort pulses. In our experiment, a mode-locked Ti:Sapphire laser (Coherent Mira 900) with a pulse width of ~ 220 fs was used as the two-photon excitation source. The experiment was performed on a home-built confocal microscope. Circular polarization was used to enable the excitation of all the GNR dimers irrespective of their random orientations in the focal plane.

By illuminating the aqueous solution of ATTO 610 with the fs laser at different wavelengths in the infrared, we got very faint fluorescence signals with spectral shape similar to the fluorescence of ATTO 610 under one-photon excitation. To verify that the emission stems from TPA, we collected the emission spectra with respect to the excitation intensity.

Fig 5.2a illustrates the power dependence of the emission spectra at the excitation wavelength of 760 nm. As is shown in Fig 5.2a, the emission spectra show little change in the shape but the intensities decrease dramatically as we reduce the excitation power. As is depicted in Fig 5.2b, the integrated intensities over the emission spectra, for both the excitation wavelengths of 760 nm and 785 nm, show a perfect quadratic dependence on the excitation power, confirming that the observed fluorescence arose from two-photon excitation for both excitation wavelengths. The broad TPA band of ATTO 610 offers us the flexibility of optimizing the collected signals by tuning the excitation wavelength and the plasmon resonance of the GNR dimers.

We performed single-molecule experiments on the assembled GNR dimers immobilized on a clean glass cover slide. The GNRs were immobilized on the glass by strong Van der Waals force after removal of all organic molecules through ozone/UV cleaning. A cross was scratched on the slide as the alignment mark to locate the positions of the observed particles for further studies. In the experiments, we chose commercial GNRs (NR-40-700, NanoSeedz) as the building blocks of the assemblies. These rods have an average diameter of 40 nm and a longitudinal plasmon mode at the wavelength of 700 nm. Simulations predict the bright plasmon mode of the end-to-end gold nanorod redshifted to ~ 760 nm after removing all the organic molecules, if we assume the interparticle separation of the dimer to be ~ 5 nm, considering the molecular size of streptavidin. Thereafter the laser wavelength of 760 nm was used as the excitation to ensure maximum enhancement. After the optical measurements, SEM images were taken to examine the structural details of the measured assemblies.

Fig 5.3 illustrates a typical single-molecule measurement of the two-photon-excited fluorescence enhanced by a GNR assembly. We first recorded the photoluminescence of each particle under excitation with the femtosecond laser, in the presence of 20 nM ATTO 610 molecules. A short-pass filter (≤ 725 nm,) was used to remove intrinsic luminescence background from the gold particles. The particles showing intensity bursts in these luminescence time traces were supposed to be the assembled structures. Indeed simulations and further experiments both show that, with enhancement by a single GNR, it is very difficult to extract single molecule fluorescence from the luminescence background of the nanorod under two photon excitation. After rinsing the sample with clean water several times, we measured the one-photon excited luminescence spectra of the particles to determine their plasmon resonances. With the help of the masked cross, we further identified the structures of these gold nanorod assemblies by comparing the SEM image with the scatter image, as one can see from the example in Fig 5.3a.

We first compared two-photon-excited fluorescence enhancement on two typical GNR dimers, assembled in either the end-to-end or the side-by-side configuration. As is shown in Fig 5.3b, for the end-to-end dimers, the plasmon resonance was red-shifted to wavelengths around 760 nm as a result of the longitudinal plasmonic coupling of each rod, while for the side-by-side structure, the plasmon resonance showed little change compared to the single GNRs. As is depicted in Fig 5.3b, for both side-by-side and end-to-end dimers, we observed the intensity bursts in the luminescence time traces. From Fig 5.3b, we can see for the maximum intensity of the bursts from the end-to-end dimer was significantly greater than those from the side-by-side structure, indicating the much larger two-photon fluorescence enhancement within the plasmonic hotspot of the end-to-end dimers. By analyzing the

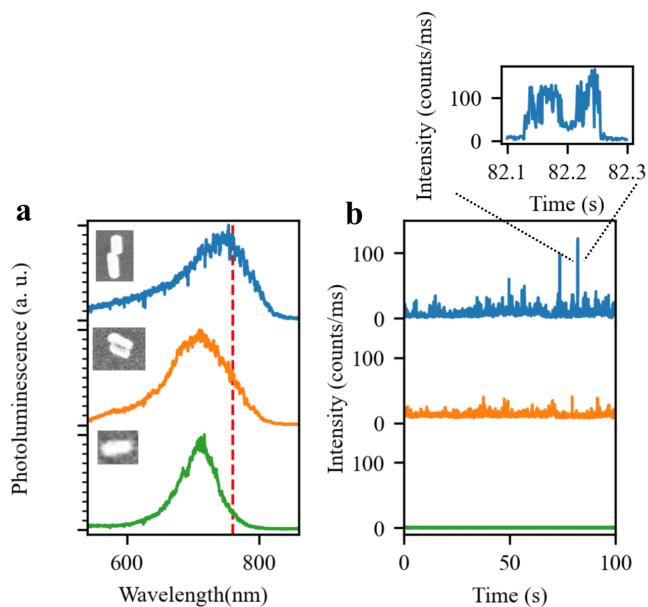


Figure 5.3: Two-photon-excited single molecule fluorescence enhancement. (a) One-photon-excited luminescence spectrum taken on three different structures made of gold nanorods: end-to-end dimer, side-by-side dimer, and a single gold nanorod, acquired under the excitation by a circular polarized 532 nm CW laser. Inset shows the SEM images of the structures. (b) The respective intensity traces taken in the presence of 20 nM ATTO 610 dyes, excited by a femtosecond laser at the wavelength of 760 nm and at the power of $\sim 2 \mu\text{W}$.

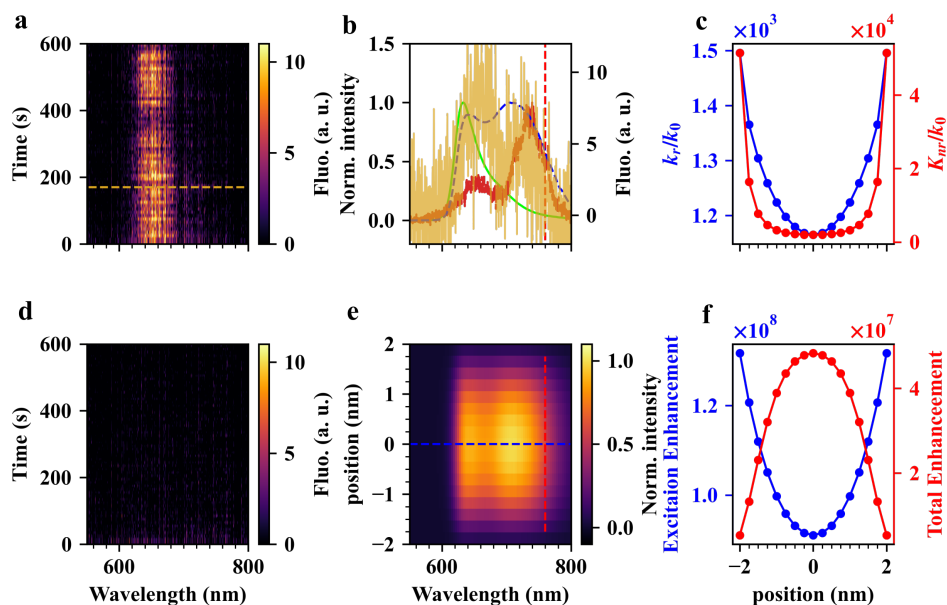


Figure 5.4: Two-photon-excited fluorescence enhancement in the plasmonic hotspot of an end-to-end gold nanorod dimer. (a) and (d) Real-time spectra on gold nanorod dimer with (a) and without (d) the presence of 100 nM ATTO 610 in solution. (b) Comparison of the measured spectrum (orange, corresponding to the recorded time of orange dashed in a) with the spectrum of free ATTO 610 dye in solution (green solid), and the simulated enhanced spectra (blue dashed, corresponding to the positions of blue dashed in e) in the hotspot. Red solid line is the scattering spectrum of the nanoparticle. (e) Simulated emission spectra of the ATTO 610 molecules at different positions along the main axis of the gold nanorod dimer in the gap. (c) Calculated radiative (blue) and non-radiative (red) enhancement factor as functions of the position in the hotspot, and (f) the respective excitation (blue) and total emission (red) enhancements. The vertical red dashed lines in (b, e) represent the wavelength of the fs laser.

highest bursts in the fluorescence time trace enhanced by the end-to-end dimer (figure 5.3b, inset), we see typical single-step single-molecule bursts with a time duration in the order of 10 ms, which confirm that the enhanced fluorescence signals are stemming from single molecules. We also notice that, as a result of the plasmon red shift, the remaining luminescence backgrounds of the end-to-end dimers, after passing through the short-pass filter, were reduced more obviously than the background of the side-by-side structure, which may further improve the single-molecule detection sensitivity of the two-photon-excited fluorescence.

Before attributing the intensity bursts to the fluorescence from single ATTO 610 molecules enhanced inside the plasmonics hotspot, we monitored the real-time spectra on the particle excited by the femtosecond laser, with/without the presence of 100 nM ATTO 610 in solution. Fig 5.4a shows one case of the real-time recording of the plasmon-enhanced two-photon-excited single-molecule emission spectra. The spectra were recorded in a time series of 10 minutes with spectral acquisition time of 10 s for each step. In the measurement, we kept the excitation power as low as possible ($\sim 0.5 \mu\text{W}$) to exclude the influence of the luminescence backgrounds from gold particles. From Fig 5.4a, we can see clearly the emission

pattern between 620 nm and 690 nm, with the intensities fluctuating over the time. Such emission pattern can be removed by replacing the ATTO 610 solution with clean water, as is shown in Fig 5.4d, which implies the signals were from ATTO 610 molecules near the particle. The spectral range, shown in figure 5.4a, was noticeably wider compared to the emission of free dyes in solution (green solid line), which was mainly due to coupling of the molecules with the plasmonic modes.

Specifically, we compare one recorded spectrum (corresponding to the dashed line in figure 5.4a) with the spectrum of the free dye (green dashed line) in figure 5.4b. The result shows drastic spectral shaping for the emission enhanced by the plasmonic nanostructure, as we can clearly see a second peak at the wavelength around 730 nm in the enhanced spectrum (orange line). This spectral shaping can be explained by the well-known effect that the far-field emission of an emitter can be modified by coupling with a plasmonic structure[38, 39], through i) the Purcell effect that enhances the spontaneous emission rate; ii) the nonradiative dissipation loss inside the metal that quenches the emission. Here, we employed a simple radiative dipole model to investigate the influence of the emission of ATTO 610 molecules by the GNR dimer. For the sake of simplicity, we considered the dimer consisting of two identical GNRs with the longitudinal axes oriented in parallel, and separated by a gap of 5 nm. More details about the simulations are given in the Supporting Information.

From Fig 5.4b, we see a good agreement between the spectral shapes of the measured emission and the simulated emission calculated at two different positions showing in Fig 5.4e (the green and blue dashed). The increase of the emission rates in the band of longer wavelength, therefore, can be attributed to the selective enhancement of the vibrational subbands in resonance with the plasmon modes. From the simulations, we also notice that the non-radiative dissipation dominates the decay rates of the excited molecule inside the gap (figure 5.4c), which quench the emission rates by a factor of about 2 in the center of the dimer (figure 5.4f). As the molecule moves closer to the gold surface, the non-radiative rate increases more than the excitation and radiative enhancements, which further reduce the fluorescence enhancement, as is shown in Figs. 5.4e and 5.4f. As a consequence, we see a maximum enhancement factor of about 5×10^7 for the two-photon-excited fluorescence at the center of the dimer.

To confirm the observed emission indeed stems from two-photon excitation, we performed a power dependence measurement on an individual GNR self-assembled nanostructure that gave single-molecule bursts. Time traces with intensity bursts excited at different powers are displayed in figure 5.5a. At the lower excitation power, as expected, we see the increase of intensity bursts as the excitation power increases. After the burst intensities reach values of about 10^2 counts/ms, we see the recorded intensity bursts is saturated as the excitation power is continually increased. This saturation might come from saturation of the molecules, or due to the plasmon damping as the result of hot electron generation, which might reduce the enhancement factor. Nonetheless, we find a quadratic dependence of the maximum fluorescence bursts on the excitation power (blue line in figure 5.5b) for the intensities below 10^5 counts/s. These maximum intensity bursts could be attributed to the signals from the molecules at the best position for enhancement. As the molecules can approach or stick to glass surface at any position inside plasmonic hotspot, with random orientations, the enhancement factor for the molecules can vary very randomly, resulting in

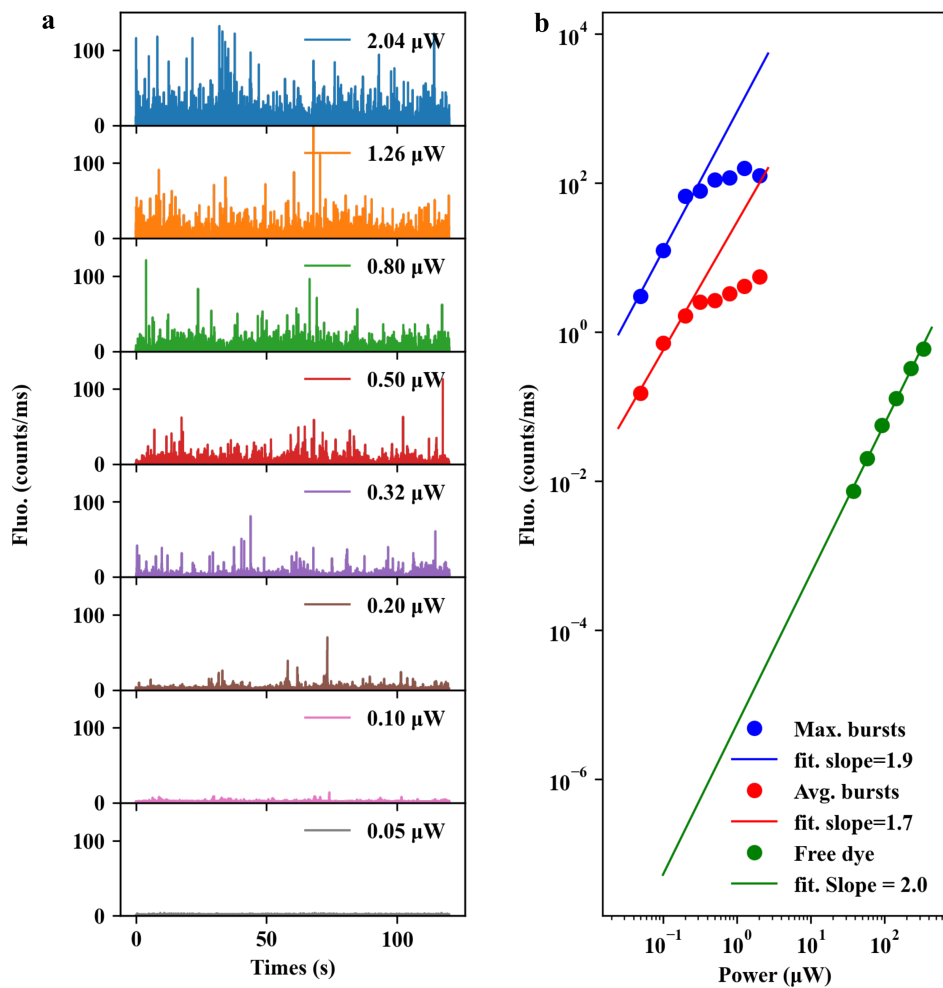


Figure 5.5: Power dependence of the emission. (a) Emission time trace (1 ms/bin) as a function of excitation power recorded on a gold nanorod self-assembled nanostructure. The particle was immersed in a solution of ATTO 610 with the concentration of 30 nM. (b) Power dependence of the maximum fluorescence burst intensity (blue), the averaged burst intensity (red), and the averaged unenhanced fluorescence per molecule.

a random distribution of intensity bursts in each time trace. This random effect can be considered by taking the average of the burst intensities for each trace. As shown in figure 5.5b, we see an approximated quadratic dependence of the averaged intensity on the excitation power with the fitted slope of 1.7 (red line).

In order to calculate the enhancement factor of the two-photon-excited fluorescence, we compared the enhanced burst intensities with the unenhanced signals from a molecule in solution. We performed power-dependent measurements for ATTO 610 molecules in the solution ($3 \mu\text{M}$) to estimate the two-photon-excited fluorescence signals excited at low power, especially for excitation below the saturation power, where the unenhanced signal in the solution is too weak to be detected. Shown in figure S5.2b, the averaged intensity of the fluorescence time trace measured in the solution (figure S5.2a) also scales quadratically with the excitation power. By taking account of the number of molecules in the focus volume, we show the quadratic dependence of the averaged fluorescence per molecule on the excitation power (green line) in figure 5.5b. By scaling the unenhanced fluorescence quadratically with the excitation power, we can estimate an enhancement factor of up to $\sim 10^8$ for the two-photon-excited fluorescence below saturation.

5.3. Conclusion

In summary, we have demonstrated the single-molecule detection of two-photon-excited fluorescence via the enhancement of self-assembled GNR dimers. In the experiment, we control the interparticle gaps by exploring the streptavidin-biotin disulfides as molecular linkers, which separate the nanorods by a distance of about 5 nm. Theoretical results indicate that two-photon-excited fluorescence rates can be enhanced by factor of up to $10^7 \sim 10^8$. With such high enhancement factor, we were able to detect the two-photon-excited fluorescence from single ATTO 610 dyes. Correlated scanning electron microscope images (SEM) were taken later to examine the configurations of the GNR dimer structures.

S5.1. Supporting Information

Assembly of gold nanorods

The GNRs were self-assembled in an end-to-end fashion through the molecular linkers based on the specific molecular recognition of biotin and streptavidin. For the assembly, a biotin disulfide solution ($20 \mu\text{M}$), EZ-link Biotin HPDP (Pierce), was pretreated with a reducing agent solution, TCEP (tris(2-carboxyethyl)phosphine), with a 1:10 biotin/TCEP ratio. This reaction was allowed at room temperature for 15 min to break the disulfide bonds in the Biotin HPDP molecules. The mixture solution was added to the streptavidin solution ($1 \mu\text{M}$) in phosphate buffered saline solution (PBS, pH = 7.4), with a ratio of 4:1 for biotin/streptavidin. The incubation lasted for 45 min to allow the binding of streptavidin with at least two biotin. The excess unbound biotin disulfide and TCEP were removed by centrifugation in centrifugal filter devices (Ultra-0.5 10K, Amicon). The residue was dispersed in $100 \mu\text{L}$ deionized water. A commercially available GNR solution (NA-40-700, OD-50, Nanoseedz) was diluted to the concentration according to its optical density (OD) of ~ 0.3 . The GNR solution had plasmon absorption at 700 nm, and the average diameter of the GNRs were 40 nm.

40 μL of a biotin-streptavidin solution was added into 500 μL as-prepared GNR solution to trigger the end-to-end assembly of the GNRs. The assembly of GNRs was monitored and recorded by a Cary 50 UV-Vis spectrometer (Varian Inc. Agilent Technology, USA) every 2 min (see figure S5.1).

Deposition of gold nanorod assemblies

When the extinction peak of the solution dropped by a ratio of 1/4, 10 μL of the GNR assembly solution was deposited onto a clean cover glass slide (Menzel-Gläser, $\phi = 25$ mm, No. 1) with a scratched cross, and was immediately covered with a second glass slide. The capillary action between the two slides squeezed the assembled solution and formed a thin layer. This strategy helps stop further assembly of GNR, and deposit the GNR assemblies uniformly on the surfaces of the glass slides. After deposition, the two slides were separated by immersing in clean water. After that, we performed UV/Ozone cleaning to remove all the organic molecules around the GNRs to ensure the proper sticking of the GNRs on the glass surface, and to create free gaps between the GNRs of the assemblies.

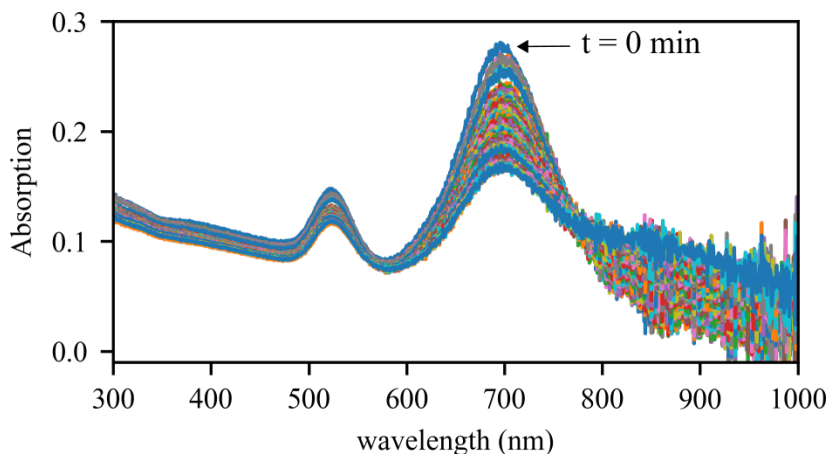


Figure S5.1: Extinction spectral evolution for gold nanorods in the presence of biotinylated streptavidin. The spectra were recorded every 2 min.

Two-photon microscopy

We performed two-photon-excited fluorescence measurements on a home-built confocal microscopy. A mode-locked titanium-sapphire laser (Coherent Mira 900), with the pulse repetition rate of 76 MHz and pulse width of ~ 220 fs, was used as the two-photon excitation source. Circular polarization was in the whole study, as it can efficiently excite all gold nanorod assemblies, regardless of their random orientations in the focal plane. The light source was focused by an oil immersion objective with a numerical aperture (NA) of 1.4. A short-pass filter (Fluorescence Edge Filter 745/SP, BrightLine) was used to separate the flu-

orescence signal from the background of scattered laser. To get the one-photon excited photoluminescence spectrum of each gold nanorod assembly, a 532 nm continuous-wave laser was used as the excitation source, and the spectrum was recorded with a liquid-nitrogen-cooled spectrometer (Acton SP-500i, Princeton Instruments). Fluorescence time traces were recorded with an avalanche photodiode (SPCM-AQRH-16, Excelitas) and processed with a time-correlated single-photon counting (TCSPC) card (TimeHarp 200, PicoQuant GmbH).

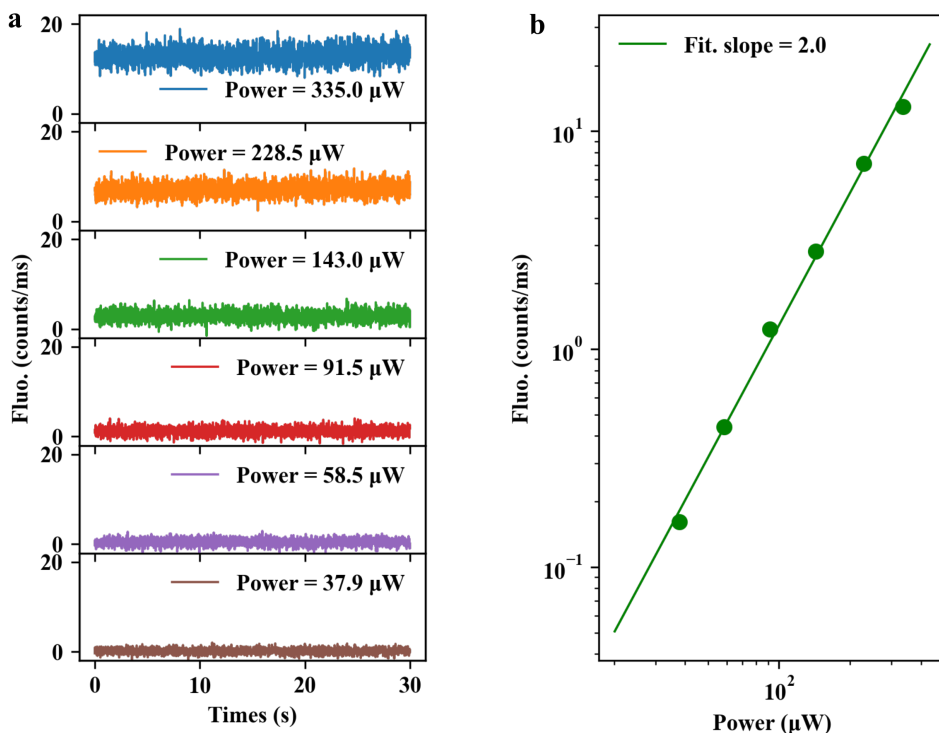


Figure S5.2: Power dependence of the emission measured in ATTO 610 solution ($3 \mu\text{M}$). (a) Fluorescence time traces excited with different laser powers. (b) Averaged fluorescence intensity as a function of the excitation power.

Two-photon-excited fluorescence of ATTO 610 in solution

We first recorded the emission spectra from the ATTO 610 solution ($\sim 5 \mu\text{M}$) excited at different laser powers. The exposure time was set as 120 s for each spectrum. In the study, we compared the power-dependent emission of ATTO 610 for two different excitation wavelengths 760 nm and 785 nm, while keeping the width and repetition rate of the pulse as constant. For both wavelengths, the integrated intensity (wavelength range from 555 nm to 728 nm) depends quadratically on the excitation power.

To estimate the average fluorescence rate of individual ATTO 610 molecules without enhancement, we performed power-dependent measurements on an ATTO 610 solution with the concentration of $3 \mu\text{M}$. Due to the extremely weak two-photon excitation efficiency

of these molecules, much higher laser power was required to get enough signal from the solution, compared to enhanced experiments. To get rid of the unavoidable background of the scattered laser at high power, we first performed power-dependent measurements in a blank solution without any dyes in it. Time traces were recorded again after replacing the water with an ATTO 610 solution at the same conditions of the blank experiments. The fluorescence signals from the molecules, therefore, can be represented by intensity time traces with molecules after subtraction of the mean intensity recorded in the blank solution (see figure S5.2a).

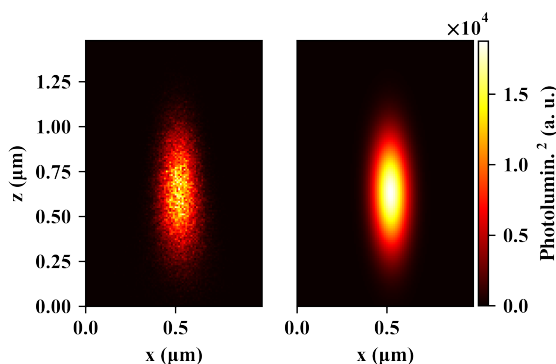


Figure S5.3: xz section of the two-photon excitation point spread function measured with a gold nanorod. Left, the xz section of the square of one-photon excited photoluminescence excited by pulse laser. Right two-dimensional Gaussian fit of the PFS, from which we get width of PSF, $\omega_x = 0.14 \mu\text{m}$ and $\omega_z = 0.42 \mu\text{m}$ and the PSF volume of $0.02 \pm 0.01 \text{ fL}$.

Figure S5.2b shows the quadratic dependence of the average fluorescence intensity measured in solution on the excitation laser power, indicating the fluorescence arose from TPA. The overall recorded signals can be simply considered as coming from the contributions of the molecules in the confocal volume.

We calculated the size of the confocal volume for two-photon excitation by measuring the confocal point spread function (PSF) of the setup. We first scanned sectional one-photon excited luminescence images of a single GNR immersed in water excited with the pulse laser. The PSF of the setup for two-photon excitation can be expressed as the square of the PSF for one photon. Shown in figure S5.3, we estimated the two-photon excitation confocal volume to be $0.02 \pm 0.01 \text{ fL}$, hence we estimate that about 20 molecules are in the upper half of the confocal volume for dye concentration of $3 \mu\text{M}$.

Numerical simulations of two-photon-excited fluorescence enhancement

We performed numerical simulations for the two-photon-excited fluorescence enhancement under weak excitation, where the excitation enhancement and the emission enhancement can be treated separately[27]. The scheme for the simulations is illustrated in figure S5.4. For the sake of simplicity, we considered the dimer consisting of two identical GNRs with the longitudinal axes oriented in parallel, and separated by a gap of 5 nm. The size of each GNR was set as $40 \text{ nm} \times 88 \text{ nm}$ to guarantee a resonance at 760 nm. The ATTO 610

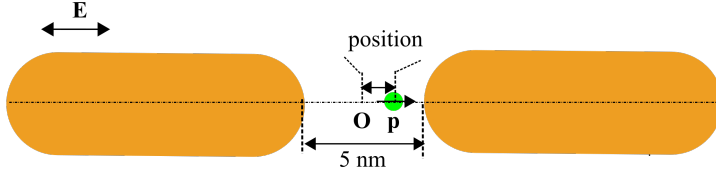


Figure S5.4: Scheme for the numerical simulations.

molecule was modeled as a radiative dipole with the position and dipole moment aligned along the longitudinal axis of the GNR dimer inside the gap. In the simulations, each GNR was modeled a spherically capped cylinder. The dielectric permittivity for gold was taken from Johnson and Christy[40], and the refractive index of the ambient medium was taken as 1.33.

For two-photon-excited fluorescence, the excitation enhancement is related to near-field enhancement as

$$\xi_{\text{exc}}^{(2)} = |\mathbf{E}|^4 / |\mathbf{E}_0|^4, \quad (\text{S5.1})$$

where (\mathbf{E}) and \mathbf{E}_0 is the (near-)field (with) and without the gold nanorod dimer.

To evaluate the enhancement factor by the GNR dimer numerically, we applied a classical electrodynamics approach based on a boundary element method (SCUFF-EM) [41, 42] to simulate the excitation and emission enhancement, respectively. To calculate the excitation enhancement, we excited the dimer structure with a plane wave with the polarization along the longitudinal axis of the dimer. The enhancement factor of the radiative rate (ξ_{rad}) and the additional non-radiative rate ($K_{\text{nr}}/k_{\text{r}}^0$) were calculated following [29, 34], where k_{r}^0 is the intrinsic radiative rate of the dye. The expected emission spectrum enhanced by the dimer can expressed as[38]

$$F(\omega) = \xi_{\text{exc}}^{(2)} \cdot f(\omega) \cdot \xi_{\text{rad}}(\omega) \cdot \frac{1/\eta_0}{\langle \xi_{\text{rad}} + K_{\text{nr}}/k_{\text{r}}^0 - 1 \rangle + 1/\eta_0}, \quad (\text{S5.2})$$

where $f(\omega)$ is the normalized emission spectrum of ATTO 610 in solution, $\langle \dots \rangle$ represents the averaging over the emission spectrum of $f(\omega)$, η_0 is the intrinsic quantum yield of the molecule, which is 0.7 for ATTO 610. The overall enhancement can be written as

$$\xi_{\text{total}} = \xi_{\text{exc}}^{(2)} \cdot \langle \xi_{\text{rad}} \rangle \cdot \frac{1/\eta_0}{\langle \xi_{\text{rad}} + K_{\text{nr}}/k_{\text{r}}^0 - 1 \rangle + 1/\eta_0}. \quad (\text{S5.3})$$

References

- [1] Peter T. C. So, Chen Y. Dong, Barry R. Masters, and Keith M. Berland. Two-Photon Excitation Fluorescence Microscopy. *Annual Review of Biomedical Engineering*, 2(1):399–429, August 2000.

- [2] Patrik R. Callis. On the theory of two-photon induced fluorescence anisotropy with application to indoles. *The Journal of Chemical Physics*, 99(1):27–37, July 1993.
- [3] Maria Göppert-Mayer. Über Elementarakte mit zwei Quantensprüngen. 401(3):273–294.
- [4] P. A. Franken, A. E. Hill, C. W. Peters, and G. Weinreich. Generation of Optical Harmonics. *Physical Review Letters*, 7(4):118–119, August 1961.
- [5] W. Kaiser and C. G. B. Garrett. Two-Photon Excitation in $\text{Ca}\{\mathrm{F}\}_2$: $\{\mathrm{Eu}\}^{2+}$. *Physical Review Letters*, 7(6):229–231, September 1961.
- [6] Patrick Theer, Mazahir T. Hasan, and Winfried Denk. Two-photon imaging to a depth of 1000 μm in living brains by use of a $\text{Ti}:\text{Al}_2\text{O}_3$ regenerative amplifier. *Optics Letters*, 28(12):1022–1024, June 2003.
- [7] Fritjof Helmchen and Winfried Denk. Deep tissue two-photon microscopy. *Nature Methods*, 2(12):932–940, December 2005.
- [8] William A. Mohler, Jeffrey S. Simske, Ellen M. Williams-Masson, Jeffrey D. Hardin, and John G. White. Dynamics and ultrastructure of developmental cell fusions in the *Caenorhabditis elegans* hypodermis. *Current Biology*, 8(19):1087–1091, September 1998.
- [9] Jayne M. Squirrell, David L. Wokosin, John G. White, and Barry D. Bavister. Long-term two-photon fluorescence imaging of mammalian embryos without compromising viability. *Nature Biotechnology*, 17(8):763–767, August 1999.
- [10] W. Denk, J. H. Strickler, and W. W. Webb. Two-photon laser scanning fluorescence microscopy. *Science*, 248(4951):73–76, April 1990.
- [11] CJ R SHEPPARD and Min Gu. Image formation in two-photon fluorescence microscopy. *Optik (Stuttgart)*, 86(3):104–106, 1990.
- [12] Min Gu and C. J. R. Sheppard. Comparison of three-dimensional imaging properties between two-photon and single-photon fluorescence microscopy. *Journal of Microscopy*, 177(2):128–137, 1995.
- [13] Shoji Maruo, Osamu Nakamura, and Satoshi Kawata. Three-dimensional microfabrication with two-photon-absorbed photopolymerization. *Optics Letters*, 22(2):132–134, January 1997.
- [14] Gilles Lemerrier, Jean-Christophe Mulatier, Cécile Martineau, Rémi Anémian, Chantal Andraud, Irène Wang, Olivier Stéphan, Nadia Amari, and Patrice Baldeck. Two-photon absorption: From optical power limiting to 3D microfabrication. *Comptes Rendus Chimie*, 8(8):1308–1316, August 2005.
- [15] Shoji Maruo and Hiroyuki Inoue. Optically driven micropump produced by three-dimensional two-photon microfabrication. *Applied Physics Letters*, 89(14):144101, October 2006.

- [16] Jin-Feng Xing, Xian-Zi Dong, Wei-Qiang Chen, Xuan-Ming Duan, Nobuyuki Takeyasu, Takuo Tanaka, and Satoshi Kawata. Improving spatial resolution of two-photon microfabrication by using photoinitiator with high initiating efficiency. *Applied Physics Letters*, 90(13):131106, March 2007.
- [17] Xiaoying Wang, Zhenping Wei, Charles Zuwu Baysah, Meiling Zheng, and Jinfeng Xing. Biomaterial-based microstructures fabricated by two-photon polymerization microfabrication technology. *RSC Advances*, 9(59):34472–34480, October 2019.
- [18] Dimitri A. Parthenopoulos and Peter M. Rentzepis. Three-Dimensional Optical Storage Memory. *Science*, 245(4920):843–845, August 1989.
- [19] James H. Strickler and Watt W. Webb. 3-D optical data storage by two-photon excitation. *Advanced Materials*, 5(6):479–481, 1993.
- [20] Shouzhi Pu, Huohong Tang, Bing Chen, Jingkun Xu, and Wenhao Huang. Photochromic diarylethene for two-photon 3D optical storage. *Materials Letters*, 60(29):3553–3557, December 2006.
- [21] A. S. Dvornikov, E. P. Walker, and P. M. Rentzepis. Two-Photon Three-Dimensional Optical Storage Memory. *The Journal of Physical Chemistry A*, 113(49):13633–13644, December 2009.
- [22] Brandon C. Marin, Su-Wen Hsu, Li Chen, Ashley Lo, Darwin W. Zwissler, Zhaowei Liu, and Andrea R. Tao. Plasmon-Enhanced Two-Photon Absorption in Photoluminescent Semiconductor Nanocrystals. *ACS Photonics*, 3(4):526–531, April 2016.
- [23] Janice B. Rabor, Koki Kawamura, Junichi Kurawaki, and Yasuro Niidome. Plasmon-enhanced two-photon excitation fluorescence of rhodamine 6G and an Eu-diketonate complex by a picosecond diode laser. *Analyst*, 144(13):4045–4050, June 2019.
- [24] Martin Bauch, Koji Toma, Mana Toma, Qingwen Zhang, and Jakub Dostalek. Plasmon-Enhanced Fluorescence Biosensors: A Review. *Plasmonics*, 9(4):781–799, August 2014.
- [25] Peter Zijlstra, Pedro M. R. Paulo, and Michel Orrit. Optical detection of single non-absorbing molecules using the surface plasmon resonance of a gold nanorod. *Nature Nanotechnology*, 7(6):379–382, June 2012.
- [26] Haifeng Yuan, Saumyakanti Khatua, Peter Zijlstra, Mustafa Yorulmaz, and Michel Orrit. Thousand-fold Enhancement of Single-Molecule Fluorescence Near a Single Gold Nanorod. *Angewandte Chemie*, 125(4):1255–1259, 2013.
- [27] Saumyakanti Khatua, Pedro M. R. Paulo, Haifeng Yuan, Ankur Gupta, Peter Zijlstra, and Michel Orrit. Resonant Plasmonic Enhancement of Single-Molecule Fluorescence by Individual Gold Nanorods. *ACS Nano*, 8(5):4440–4449, May 2014.
- [28] Weichun Zhang, Martín Calderola, Xuxing Lu, Biswajit Pradhan, and Michel Orrit. Single-molecule fluorescence enhancement of a near-infrared dye by gold nanorods using DNA transient binding. *Physical Chemistry Chemical Physics*, 20(31):20468–20475, 2018.

- [29] Xuxing Lu, Gang Ye, Deep Punj, Ryan C. Chiechi, and Michel Orrit. Quantum Yield Limits for the Detection of Single-Molecule Fluorescence Enhancement by a Gold Nanorod. *ACS Photonics*, 7(9):2498–2505, September 2020.
- [30] Alexandra P. Francisco, David Botequim, Duarte M. F. Prazeres, Vanda V. Serra, Sílvia M. B. Costa, César A. T. Laia, and Pedro M. R. Paulo. Extreme Enhancement of Single-Molecule Fluorescence from Porphyrins Induced by Gold Nanodimer Antennas. *The Journal of Physical Chemistry Letters*, 10(7):1542–1549, April 2019.
- [31] Tianyue Zhang, Guowei Lu, Jie Liu, Hongming Shen, Pascal Perriat, Matteo Martini, Olivier Tillement, and Qihuang Gong. Strong two-photon fluorescence enhanced jointly by dipolar and quadrupolar modes of a single plasmonic nanostructure. *Applied Physics Letters*, 101(5):051109, July 2012.
- [32] Ding-Feng Zhang, Shuang Li, Qing-Hua Xu, and Yong Cao. Aggregation-Induced Plasmon Coupling-Enhanced One- and Two-Photon Excitation Fluorescence by Silver Nanoparticles. *Langmuir*, 36(17):4721–4727, May 2020.
- [33] Russell A. Jensen, I-Chun Huang, Ou Chen, Jennifer T. Choy, Thomas S. Bischof, Marko Lončar, and Mounqi G. Bawendi. Optical Trapping and Two-Photon Excitation of Colloidal Quantum Dots Using Bowtie Apertures. *ACS Photonics*, 3(3):423–427, March 2016.
- [34] Weichun Zhang, Martín Caldarola, Xuxing Lu, and Michel Orrit. Plasmonic Enhancement of Two-Photon-Excited Luminescence of Single Quantum Dots by Individual Gold Nanorods. *ACS Photonics*, 5(7):2960–2968, July 2018.
- [35] Oluwafemi S. Ojambati, Rohit Chikkaraddy, William M. Deacon, Junyang Huang, Demelza Wright, and Jeremy J. Baumberg. Efficient Generation of Two-Photon Excited Phosphorescence from Molecules in Plasmonic Nanocavities. *Nano Letters*, 20(6):4653–4658, June 2020.
- [36] J. Mertz, C. Xu, and W. W. Webb. Single-molecule detection by two-photon-excited fluorescence. *Optics Letters*, 20(24):2532–2534, December 1995.
- [37] K. K. Caswell, James N. Wilson, Uwe H. F. Bunz, and Catherine J. Murphy. Preferential End-to-End Assembly of Gold Nanorods by Biotin-Streptavidin Connectors. *Journal of the American Chemical Society*, 125(46):13914–13915, November 2003.
- [38] M. Ringler, A. Schwemer, M. Wunderlich, A. Nichtl, K. Kürzinger, T. A. Klar, and J. Feldmann. Shaping Emission Spectra of Fluorescent Molecules with Single Plasmonic Nanoresonators. *Physical Review Letters*, 100(20):203002, May 2008.
- [39] G. Vecchi, V. Giannini, and J. Gómez Rivas. Shaping the Fluorescent Emission by Lattice Resonances in Plasmonic Crystals of Nanoantennas. *Physical Review Letters*, 102(14):146807, April 2009.
- [40] P. B. Johnson and R. W. Christy. Optical Constants of the Noble Metals. *Physical Review B*, 6(12):4370–4379, December 1972.

- [41] M. T. Homer Reid and S. G. Johnson. Efficient Computation of Power, Force, and Torque in BEM Scattering Calculations. *ArXiv e-prints*, July 2013.
- [42] <http://github.com/homerreid/scuff-EM>.